



**Repositorio Institucional de la Universidad Autónoma de Madrid**

<https://repositorio.uam.es>

Esta es la **versión de autor** del artículo publicado en:  
This is an **author produced version** of a paper published in:

Applied Geochemistry (2020): 23 April

**DOI:** <https://doi.org/10.1016/j.apgeochem.2020.104599>

**Copyright:** © 2020 Elsevier

El acceso a la versión del editor puede requerir la suscripción del recurso

Access to the published version may require subscription

## Bentonite/CEM-II cement mortar INTERFACE EXPERIMENTS: a proxy to in situ deep geological repository engineered barrier system surface reactivity

Daniel E. González-Santamaría<sup>1\*</sup>, Raúl Fernández<sup>1</sup>, Ana. I. Ruiz<sup>1</sup>, Almudena Ortega<sup>1</sup>, Jaime Cuevas<sup>1</sup>

<sup>1</sup>Department of Geology and Geochemistry, Faculty of Sciences, Autonomous University of Madrid, Cantoblanco, 28049, Madrid, Spain

\*Corresponding author: daniel.g.santamaria@uam.es, ORCID iD: 0000-0002-1175-9763

Telephone: +34 91 497 5769

### Abstract

The present study focuses on the interaction between cement mortar (OPC-based CEM-II) and the FEBEX-bentonite; this interaction takes place at a small spatial scale (~1 cm/~1 cm; compacted cement mortar/compacted bentonite thickness) within a timeline of 6 and 18 months. This work was designed to determine the early interaction processes and compare them with large-scale FEBEX *in situ* underground research laboratory experiments. The study aimed at the primary reactions that occurred at the interface in a small spatial scale (nm- $\mu$ m scale). The experimental device consisted of a composite column containing the cement mortar/bentonite materials. A granitic groundwater solution was injected through the cement mortar/bentonite system and collected out of the column in sequential syringes for analysis of the chemical composition evolution. For the study of the post-mortem samples, an innovative use of grazing incidence X-ray diffraction was performed to determine the phases produced at the interface. Scanning electron microscopy coupled to energy dispersive X-rays and local specific surface area measurements were also applied. The main results showed the initial development of a Mg perturbation in FEBEX-bentonite at the interface related to the formation of 7 Å precursors of Mg-clay 2:1 sheet silicates as the main neogenic phases expected in the long term. Additionally, a Ca-carbonation skin (calcite) occurred in cement mortar at the interface. The specifications of the reaction products observed at small scales of time and space ( $\mu$ m) are highly promising for the development of reaction concepts and support modelling in the future, which could offer a useful perspective for advancement in the upscaling of concrete/bentonite interface perturbation.

**Keywords:** deep geological repository, alkaline alteration upscaling, engineered barrier system, cement-bentonite interface, carbonation, Mg silicates hydrates.

### Highlights

Cement mortar/bentonite interface reactions occur at short time and small spatial scale

Mg perturbations are visible in bentonite due to the formation of Mg silicates hydrates

Calcite crusts at the interface occur from decalcification in the cement matrix

Al migration from bentonite promotes the formation of ettringite and C-A-S-H into the cement

The specific surface area increases next to the interface

## 1 Introduction

In recent decades, concern related to high-level radioactive waste (HLRW) management has been growing. HLRW, mostly spent fuel, is presently safely hosted within the facilities of nuclear power plants but its storage at long term requires international consensus based on the safest technical and scientific practices due to its long-lived radiotoxicity ( $10^4$ - $10^5$  years). Currently, the deep geological repository (DGR) is considered as the best solution for long-term isolation of HLRW to avoid its release to the biosphere. The DGR is based on a multiple engineered barrier system (EBS), which is placed in a host rock formation (Ewing et al., 2016). Concrete and bentonite are two main components of the EBS when considering granitic bedrock for a DGR. Those materials are exposed to the groundwater from the granite, whose composition depends on the characteristics of each site. Cementitious materials produce alkaline pore fluids with a pH from 10 to 13.5 (Berner, 1992), in contrast with the almost neutral pH of bentonite. This disequilibrium results in geochemical reactions that progress at changing rates during the entire life span of the facility. It is crucial to assure the safety of EBS and to gain full knowledge of the key reaction pathways involved from the initial stages to understand its evolution in the long term. For this reason, efforts are being made to evaluate those disturbances and their evolution at different spatial scale (from small laboratory to real size *in-situ* experiments) and temporal scale (from a few months to over decades). Several approaches are underway, and pertinent knowledge is expected from the study of clay reactions in natural alkaline environments as natural reactivity analogues (Khouri et al., 1985; Savage, 2011). Long-term concrete/bentonite systems studies at repository scale are available throughout experiments performed in underground research laboratories (URLs). URLs are essential to supplying scientific and technical data from several years to decades of reaction to the real spatial scale of a repository.

The results of cement/clay interaction from large-scale facilities usually offer instant pictures of the resulting reactivity that characterizes interfaces after long periods of time (e.g. Fernández et al., 2018; Tinseau et al., 2006). However, the interpretation of results is not always straightforward because, due to the large dimensions, the

reactivity is heterogeneous. Therefore, knowledge acquired on the reactivity by homogeneous laboratory scale experiments is useful to interpret and predict the reactivity at long-term (Cuevas et al., 2018a).

The state-of-the-art on the alkaline alteration of bentonite has been well described by Dauzères et al. (2010) and reviewed by Gaucher and Blanc (2006) and Savage et al. (2007).

Short-term laboratory-based experiments enable to study different materials in virtually equal controlled conditions in order to compare their behaviour, what is relevant to determine the most suited materials to be implemented, which is currently a discussion issue (González-Santamaría et al., 2018). For example, low-pH cement-base materials ( $\text{pH} < 12$ ) were proposed to avoid the extreme alkalinity (Berner et al., 2013) and García-Calvo et al. (2010) demonstrated their resistance to granitic groundwater exposure after 2 years of interaction. In contrast, under the influence of carbonated water, low-pH cements exhibit lower resistance than that of high-pH cements (Dauzères et al., 2016), and hydration products such as ettringite are more unstable (Trotignon et al., 2007). The present short-term experiments might be able to supply complementary data on the early stage of geochemical interactions and evidence for reactions that are implemented in geochemical modelling (Churakov and Prasianakis, 2018). Additionally, this information can aid in the upscaling of processes that take place from months to decades.

This study focuses on the interactions of cement mortar with CEM II (hereafter referred to as cement mortar or CEM II-C) and FEBEX-bentonite. Our objective is to be able to compare materials interactions similar to those observed after 13 years from the dismantling of the FEBEX *in situ* experiment at the granitic Grimsel Test Site (GTS) URL in Switzerland (Fernández et al., 2017). The FEBEX *in situ* experiment simulated thermo-hydro-mechanical and chemical conditions of a DGR by substituting radioactive waste containers for two metallic heaters. The experiment lasted 18 years but one heater was switched off after 5 years and then extracted. The emptied part of the gallery was sealed with a sprayed concrete plug that remained in contact with the compacted bentonite barrier for the next 13 years until the final dismantling. The methodological approach of the present study is based on the previous procedures developed in a pilot project to study the geochemical reactions on a short-term scale (González-Santamaría et al., 2018).

The experiments performed in this work have been designed to detect early reactions at the interface in a small range extension (nm- $\mu\text{m}$  scale) and have been practised in a composite column containing the cement mortar-bentonite (CB) materials. The innovative use of grazing incidence X-ray diffraction (GI-XRD) and  $\theta$ -2 $\theta$  scans on the solid post-mortem samples has been applied to determine the phases produced at the immediate interface of cement mortar and bentonite. The different X-ray diffraction (XRD) techniques applied have been combined with complementary scanning electron microscopy coupled to energy dispersive X-rays (SEM-EDX) and local specific

surface area (SSA) measurements. In addition, the effluent displaced out of the column has been determined to study the evolution of the aqueous chemical composition.

## 2 Methods

### 2.1. Experimental setup

Cured cement mortar and FEBEX-bentonite (compacted at a dry density of  $1.6 \text{ g/cm}^3$ ) were placed in a methacrylate cylindrical sleeve confined by two stainless steel caps, which constitute a transport cell, and separated by a  $0.45 \text{ }\mu\text{m}$  polytetrafluoroethylene (PTFE) membrane (Fig. 1). The cell dimensions were 20 mm in internal diameter and 9 mm in height for each material (18 mm in total). The objective of the design was ease of dismantling of the transport cells for further solid characterization, thus allowing the rapid separation of cement mortar and bentonite from the carcass. This design prevented deformation and drying of both materials and also avoided atmospheric interaction. The compact external stainless-steel case (together with connections and filters) was able to resist the high-pressure conditions caused by the hydration of bentonite (Villar and Lloret, 2004). In accordance with the *in situ* conditions at the GTS (Alonso et al., 2017; Fernández et al., 2017), granitic groundwater was injected at a constant 1 MPa hydraulic head through PEEK tubes using an automatic piston pump (Gilson, 307 model). The effluent volume was measured and collected at the bentonite end.

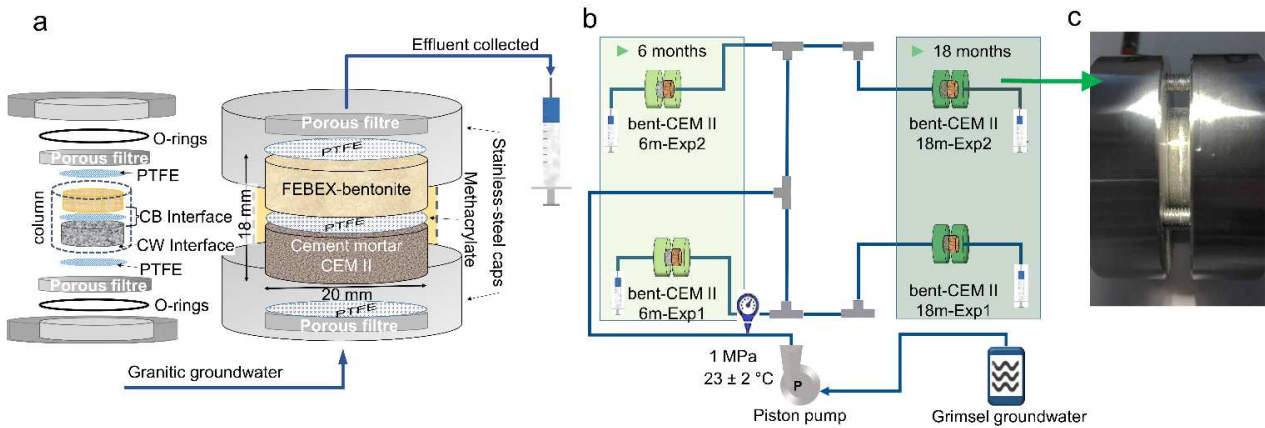


**Fig. 1.** Design of the transport cells. (a) Transport cells formed by cement mortar/compacted bentonite separated by a PTFE membrane and encased in an open stainless-steel sleeve. A methacrylate cylinder contains the column. Two porous filters allow water transport at both column ends. CB: cement mortar-bentonite interface; CW: cement-water interface. (b) it is represented the experimental scheme of the duplicated cells at two different periods: 6 and 18 months. ben: FEBEX-bentonite, CEM II. Cement mortar with CEM II as ordinary Portland cement (OPC). (c) Photograph of one of the transport cells.

Two duplicated transport cells were run for 6 months, and the other two cells were run for 18 months, under virtually isothermal laboratory conditions ( $23 \pm 2$  °C). In fact, this condition is similar to the temperatures expected at the concrete bentonite interface, according to the data obtained from the FEBEX *in situ* experiment (Villar et al., 2012).

## 2.2. Sampling procedures (subsamples sectioning)

After the experiments were run, the cement mortar-bentonite columns were dismantled and divided into several samples using a cutting machine (Well®2000 model) with a diamond wire saw (Fig. 2) that allows to cut in dry conditions without heating the sample. The cut is slow and the sample is covered with parafilm to protect any interaction with the atmospheric air. The aim was to identify the presence of newly formed mineral phases at the CB-interface by studying the surfaces of the C1 and B1 slices, and the CW-interface was also studied in the external surface of the C3 slice (Fig. 2b) via SEM-EDX.

To assess the evolution of the materials in terms of distances, subsamples with 3 mm thickness sliced parallel to the interface were cut (Fig. 2b) for XRD and SSA analyses. After vacuum drying and grinding, cement mortar samples were stored in a hermetic chamber in the presence of NaOH lentils to prevent absorption of CO<sub>2</sub> by the cement-mortar, at a relative humidity (R. H.) <10%. The FEBEX-bentonite slices were also ground and equilibrated in 50% R. H. before XRD analysis to rehydrate the exchangeable cations and stabilize the smectite basal spacing.

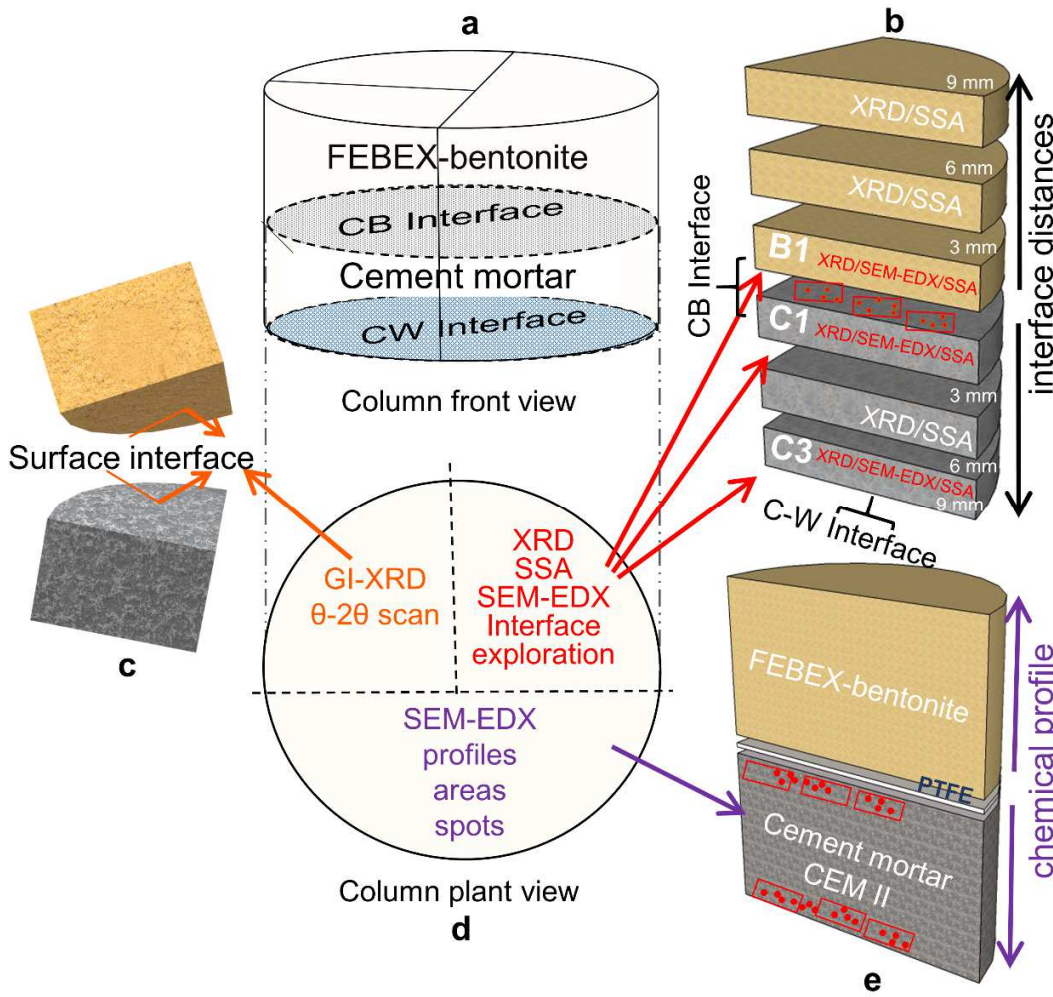


**Fig. 2.** Cutting and sampling scheme. (a) Front view with CB-interface and the CW-interface drawn (grey and blue ellipses). (b) Sample segmentation for XRD, SSA measurements and previous SEM-EDX exploration of the surface interfaces in slices B1, C1 and C3. (c) Sample quarter for GI-XRD and  $\theta$ -2 $\theta$  scans. (d) Plan view of the column. (e) Half column cut to show both the complete profile and also areas and punctual analysis next to the CB and CW-interfaces by SEM-EDX.

GI-XRD and  $\theta$ -2 $\theta$  scans of the cement and bentonite interfaces (facing the PTFE membrane) were conducted on one of the cut quarters (Fig. 2c). The remaining flat surface of the half column perpendicular to the interface (Fig. 2e) was polished after freeze-drying treatment and was subsequently embedded in epoxy resin. Epoxy resin does not enter the materials and serves as a protective framework to confine the sample without destroying its integrity during the polishing operation, although the freeze-drying process can destabilize ettringite and other cement hydrates. After polishing, the sample was prepared for elemental chemical profiling via SEM-EDX. The linear transect selected to determine the elemental composition profile of the entire column was obtained using the CB-



interface as the origin of distance coordinates. EDX measurements were collected towards the bentonite end of the column and towards the interface with the infiltrating groundwater solution (CW-interface) crossing the cement mortar. These analyses were performed in additional detail next to the CB-interface, with area dimensions of  $10\text{ }\mu\text{m height} \times 100\text{ }\mu\text{m width}$  in the direction perpendicular to the CB-interface. The following 5 analysis were executed with dimensions of  $\sim 50\text{ }\mu\text{m} \times 500\text{ }\mu\text{m}$ , followed by 7 and 16 analysis towards the bentonite column end and 10 analysis towards the CW-interface with dimensions of  $100\text{ }\mu\text{m} \times 1200\text{ }\mu\text{m}$  and  $500\text{ }\mu\text{m} \times 3000\text{ }\mu\text{m}$ , respectively. A similar methodology can be found in González-Santamaría et al. (2018) and Fernández et al. (2017). A schematic sketch of the number of analyses and increasing areas is shown in the latter paper.

In the same half sample (Fig. 2e), the CEM II-C side was analysed as follows. Three rectangular areas of approximately  $1\text{ mm}^2$  were registered for major element quantification near the CB and CW-interfaces (Fig. 3a). Within these areas, punctual (also referred as spot) EDX analyses of the cement matrix were conducted at 200x magnification, and at least 7 spots were acquired in representative fields for the cement matrix (Fig. 3b).

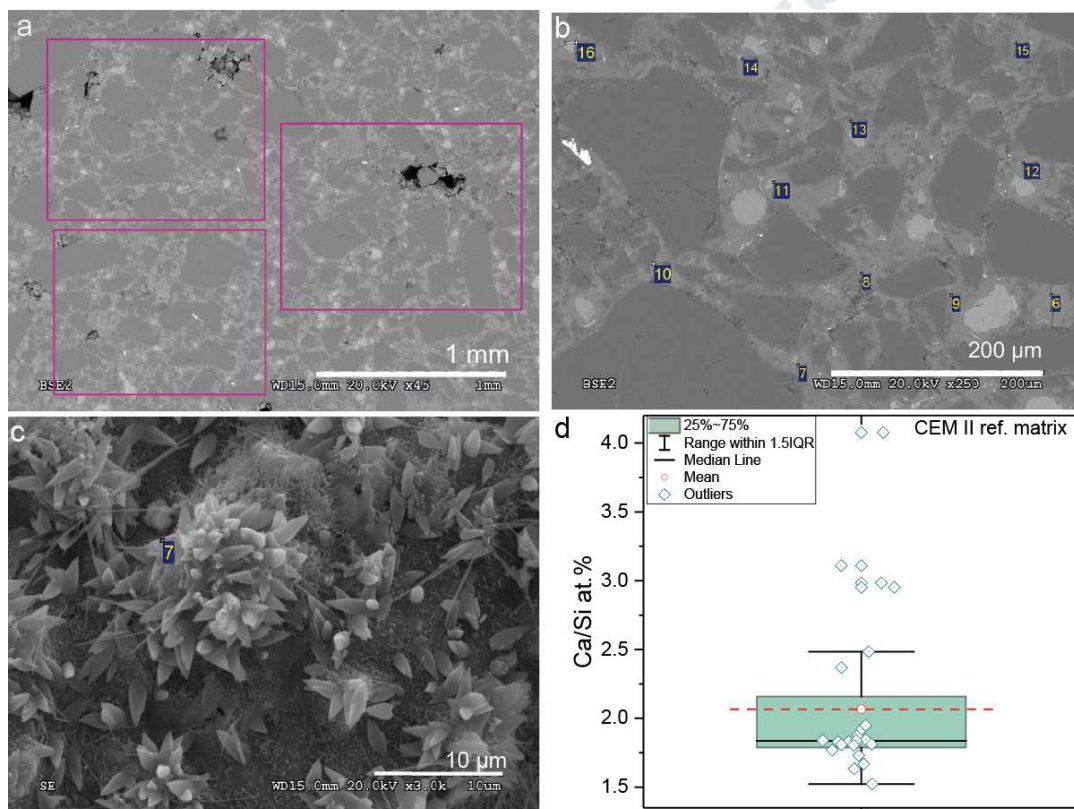




**Fig. 3.** SEM backscattering images from (a) area analyses conducted at 45x magnification, (b) matrix spot analysis locations conducted at 200x magnification and (c) micrograph in which calcium carbonate (bi-sphenoids) and ettringite needles are supported in the C-S-H cement matrix, and (d) statistical analysis of the Ca/Si atom ratio in the cement matrix.

### 2.3. Analytical techniques

XRD analysis of randomly oriented cement mortar and bentonite powders (samples shown in Fig. 2b) were conducted using a  $\theta$ -2 $\theta$  X'Pert PANalytical instrument with an X'Celerator detector. XRD patterns were recorded in an angular range of 3-70° 2 $\theta$ . The detector allowed measurements equivalent to 0.016° angular steps for 100 s at each step. The voltage and intensity of the operated X-ray Cu tube were 45 kV and 40 mA, respectively. Complementarily, the GI-XRD analysis and  $\theta$ -2 $\theta$  scans were performed at both surfaces of the CB-interface (samples shown in Fig. 2c) to assess the perturbation that occurred in the first microns. The GI-XRD was configured with a fixed incidence angle of 0.5° 2 $\theta$ . Both measurements were performed using 0.04° and 2 seconds of angular step and time step increases, respectively. Finally, the angular range recorded was 3-70° 2 $\theta$ .

The SEM-EDX equipment was run on a Hitachi S-3000N scanning electron microscope coupled to an INCAx-sight Oxford Instruments™ energy-dispersive X-ray analyser. EDX semi-quantification of major elements was performed using internal standard semi-quantitative analysis. The statistical quality of elemental concentrations is detailed in (González-Santamaría et al., 2018). In summary, on the cement mortar side and for elements > 20% (Al, Si, Ca), the instrumental % deviations obtained were less than 10% because their concentrations were lower for silicon (<1%), Ca (<5%) and higher for Al (9%). For elements with contents within 1–5% (Mg, Ca, K, Fe), the percentage of deviation from the average of the measured values was typically 10–15%. Punctual analysis acquired in EDX areas or spots acquired for characterizing cement matrix or phase composition were treated with IBM® SPSS® Statistic software. Test one-way ANOVA, multiple comparisons (Post Hoc Test) and test Kruskal-Wallis (p-value<0.05) were done to compare the different groups of experiments.

Specific surface area (SSA) was measured by means Gemini V porosimeter Micromeritics® equipment to relate the external surface and size of particles present in the materials. The technique is based on the method of adsorption of N<sub>2</sub>(g) as analysed by the Brunauer, Emmett and Teller (BET) equation (Webb and Orr, 1997). Bentonite samples were heated at 90 °C for 24 h in a sample holder and then outgassed in a nitrogen current for 2 h in a degasification station before measurement, as in Cuevas et al. (2016). However, cement mortar samples were only heated for 2 h, instead of 24 h, to prevent dehydration of hydrated cement phases.

The aqueous effluent parameters picked up by the disc in the disposed syringe were analysed using a Metrohm 888™ automated potentiometric titration device for measurement of pH and alkalinity. Silica was determined by visible spectrophotometry using the molybdate blue complex method in a Milton Roy Spectronic® instrument at a

wavelength of 825 nm. The major chemical ions were analysed with ion chromatography equipment coupled to a conductivity detector (IC-CD) using a Metrohm 802 compact IC plus model. Additionally, the hydraulic conductivity was also calculated for each transport cell by periodical weighing of the collection syringes to measure the flow rate and applying the Darcy's law.

### 3 Materials

#### 3.1. Granitic groundwater

The main characteristics of the groundwater obtained from the GTS are its notably diluted composition of  $\text{Na}^+$ ,  $\text{Ca}^{2+}$ ,  $\text{HCO}_3^-$ ,  $\text{Cl}^-$ , and  $\text{SO}_4^{2-}$  ions. GTS-groundwater has a value of  $104 \mu\text{S}/\text{cm}$  for electrical conductivity, and the main ions concentrations (mg/L) are  $\text{Cl}^-$  (3.5),  $\text{SO}_4^{2-}$  (9.6),  $\text{HCO}_3^-$  (42.7),  $\text{Na}^+$  (11.5),  $\text{K}^+$  ( $<0.1$ ),  $\text{Ca}^{2+}$  (12.0), and  $\text{Mg}^{2+}$  ( $<0.1$ ), with a pH of 8.1 (Garralón et al., 2017).

#### 3.2. FEBEX-bentonite

FEBEX-bentonite was obtained from the Cortijo de Archidona deposits (Caballero et al., 2005) and contains more than 90% montmorillonite (Mnt) and variable quantities of quartz (qtz;  $2 \pm 1$ ), plagioclase (pl;  $3 \pm 1$ ), K-feldspar (Kfp;  $< 1$ ), calcite (Cal;  $< 1$ ) and cristobalite (Crs;  $2 \pm 1$ ). The FEBEX-bentonite contains approximately 1/3, 1/3 and 1/4 cmol (+ charge)/kg of  $\text{Mg}^{2+}$ ,  $\text{Ca}^{2+}$  and  $\text{Na}^+$  exchangeable cations, respectively, for a cation exchange capacity (CEC) of  $102 \pm 2$  cmol(+)/kg. The physical-chemical properties of the FEBEX bentonite and its most relevant thermo-hydro-mechanical and geochemical properties have been studied and are published elsewhere (e.g. Villar et al., 2006).

The bentonite, milled to a grain size  $< 1$  mm, was compacted with its hygroscopic water content (13 wt.%) at room temperature conditions ( $23 \pm 2^\circ\text{C}$ ) and at a nominal dry density of  $1.60 \text{ g}/\text{cm}^3$  inside the methacrylate sleeve, where the cement mortar was previously hardened.

#### 3.3. Cement mortar

Cement mortar was prepared with CEM II/A-L 42.5 R SR cement formulated with powder limestone addition (10%). Subsequently, a 1/2.4 ratio of distilled water/cement and a 1/3 ratio of cement/silica sand (grain size  $< 1$  mm; 99% of quartz) were added. The materials used to prepare the CEM II-C were supplied by the Eduardo Torroja Institute for Construction Science (CSIC-IETcc) and were cast inside a methacrylate sleeve, uniaxially pressed at  $1\text{--}2 \text{ kg}/\text{cm}^2$  and covered by pressing of a circular PTFE porous membrane. The cast CEM II-C was

cured in a water-saturated chamber (100% R. H.) for 90 days. After the CEM II-C was cured, the compacted FEBEX-bentonite was emplaced.

The SSA of the cement mortar was  $9.3 \pm 0.1 \text{ m}^2/\text{g}$ , and the pH value measured in the pore solution following the ex situ method of (García Calvo, 2012) was  $12.2 \pm 0.1$ .

To obtain an initial reference sample, the CEM II-C was prepared and characterized in manner similar to that of the other experimental samples.

The average elemental composition obtained by EDX analyses of the areas acquired at 45x magnification (approximately  $1 \text{ mm}^2$ ) and the matrix punctual analyses acquired at 200x magnification are shown in Table 1. See that punctual analyses exclude mortar aggregates, mainly quartz grains, and consequently the Si content decreases in the cement matrix, increasing thereby the rest of elements.

**Table 1.** Chemical composition of CEM II cement mortar (CEM II-C) and average composition of cement matrix. Major elements are recalculated to 100%

At. %	Areas at 45x mag;	Matrix at 200x mag
	Mean $\pm$ Sx (3-5 areas)	Mean $\pm$ Sx (7 spots)
Mg	n.d.	n.d.
Al	$2.36 \pm 0.30$	$3.54 \pm 2.85$
Si	$74.70 \pm 1.29$	$30.62 \pm 6.75$
S	$1.24 \pm 0.39$	$2.26 \pm 0.76$
K	n.d.	n.d.
Ca	$20.46 \pm 1.01$	$60.39 \pm 7.56$
Fe	$0.65 \pm 0.09$	$0.85 \pm 0.54$

Sx: Standard deviation, At. %: atomic percentage, mag: magnification, n.d.: not detected  
Areas and matrix analyses are shown in Fig. 3a-b.

The XRD powder patterns showed the presence of calcite, gypsum, quartz, and phases commonly present in the hydrated cement, namely, portlandite, ettringite, ferrite and dicalcium/tricalcium silicate anhydrous phases (see section 4.3). Calcium silicate hydrates (C-S-H) are the major hydration products and binding phases in cements, but they were not detected by XRD because they do not diffract well (Techer et al., 2012). Instead, C-S-H were observed by SEM-EDX as nano-crystalline phases, mostly identified by their chemical composition because the SEM resolution do not reach the nm scale.

The presence of anhydrous phases determined by XRD is coherent with the analysis conducted at 200x magnifications for the characterization of cement mortar matrix. The median Ca/Si ratio based on 26 analyses ranged from  $\sim 1.7$  to 2.0 (Fig. 3d). In general, this ratio indicates an excess of Ca, overestimated due to the size of

the microanalysis area and the existence of limestone microparticles (Alonso et al., 2017). Several determinations exceed a Ca/Si ratio of 2.3 that clearly indicates that contribution. The SEM-EDX exploration confirmed a combination of phases determined by the presence of ettringite, portlandite, calcium carbonate (identified as calcite by XRD), and C-S-H (Fig. 3).

## 4 Results

### 4.1. SEM-EDX

#### 4.1.1. SEM-EDX 45x (bulk cement mortar) and 200x (cement mortar matrix) analysis areas

Only the cement mortar side was analysed at 45x and 200x magnification because the bentonite composition is rather homogenous under area or spot analyses, and its variation is better described by EDX elemental profiles (see section 4.1.2). The area and spot measurements performed on the CEM II-C were acquired to assess the evolution of the entire cement mortar material and the matrix of the cement mortar, respectively. The data from the duplicated cells were grouped into 6 and 18 months, representing averaged values for each experiment.

The bulk cement mortar compositions acquired from area analyses at the CB or CW-interfaces after interaction are compared with the composition of the reference cement mortar in Table 2. The CB-interface shows a significant decrease in Ca and Si after 6 months. Conversely, Ca increases again up to the initial values after 18 months. In the CW-interface, Ca leaching after 6 months is not important and highly variable. Additionally, Mg is detected in the composition after 18 months at both the CB and CW-interfaces. Overall, no statistically significant differences were observed with respect to the area analyses.

**Table 2.** EDX area analyses performed at different time-scales (0, 6 and 18 months) and interfaces (CB and CW). Averaged values include standard deviations.

Values include standard deviations.					
	Reference	CB-interface		CW-interface	
Element (At.%)	0 months	6 months	18 months	6 months	18 months
Mg	n.d.	n.d.	0.28 ± 0.16	n.d.	0.24 ± 0.13
Al	2.36 ± 0.30	2.54 ± 0.85	2.48 ± 0.38	1.58 ± 0.43	2.39 ± 0.31
Si	74.70 ± 1.29	80.08 ± 2.87	74.10 ± 2.10	77.31 ± 4.48	72.88 ± 4.07
S	1.24 ± 0.39	0.76 ± 0.39	1.47 ± 0.39	0.86 ± 0.21	1.12 ± 0.37
K	n.d.	n.d.	n.d.	n.d.	n.d.
Ca	20.46 ± 1.01	15.54 ± 2.27	20.90 ± 1.44	19.09 ± 4.77	22.60 ± 3.44
Fe	0.65 ± 0.09	0.76 ± 0.26	0.76 ± 0.14	0.88 ± 0.16	0.73 ± 0.29

At.%: atomic percentage, n.d.: not detected.

At the CB-interface, the cement mortar matrix compositions showed an averaged significant decrease in the Ca/Si ratio from the reference (0 months;  $\sim 1.8$ ) to 6 months ( $\sim 1.5$ ). After 6 months, this parameter remained stable until 18 months (Fig. 4a). Independently of the time of reaction, the Ca/Si displays a spread of values from 1.2 to 1.8, showing an uneven degree of hydration and decalcification of C-S-H. The spread of the Ca/Si ratio data is slightly larger after 18 months, with notably high values ( $> 2$ ), presumably due to calcite precipitation. In contrast, values  $< 1.0$ -0.6 are more typical of low Ca/Si tobermorite, C-S-H or C-A-S-H. The presence of C-A-S-H is detected in the CB-interface with Al/Si ratios that are clearly higher than in the reference cement mortar matrix (Fig. 4b).

At the CW-interface, the Ca/Si ratio does not decrease at the same rate as at the CB-interface. The slightly decreasing shift from 0 to 6 months and from 6 to 18 months is consistent with the presence of hydrated and lower Ca/Si C-S-H phases. Both interfaces show more dispersed data for the cement matrix than the reference.

The differences in distribution of Al/Si (Fig. 4b) were significant across categories of interfaces (CB-CW-interface) but not significant across the time scale (6 and 18 months experiments).

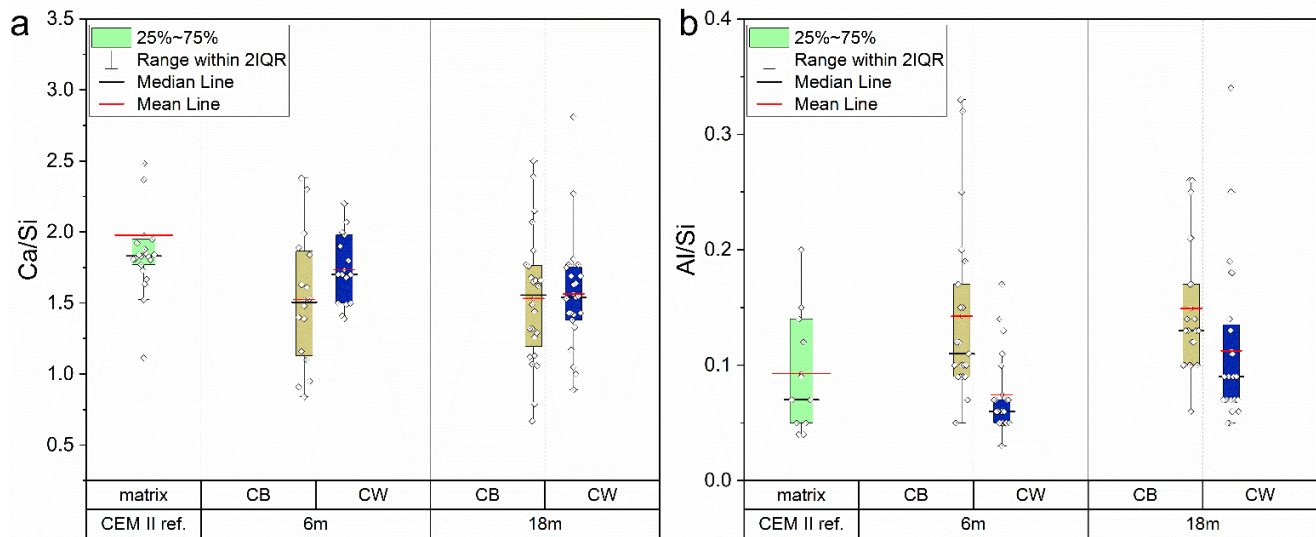


**Fig. 4.** Box plot of the Ca/Si ratios (a) and Al/Si ratios (b) analysed in the matrix of the cement mortar. Horizontal black lines inside the box charts represent the median value of the data. Colour boxes indicate the values contained within the 25-75% interquartile range (IQR), the range of the vertical bars extent to 2 IQR, median line is shown in black and mean line in red.

#### 4.1.2. SEM-EDX profiles of chemical composition in cement mortar and bentonite

The chemical evolution of Si, Ca, Al and Mg as a function of time (6 and 12 months) in cement mortar and bentonite is presented in Fig. 5a. In general, the Ca content shows a maximum on the cement mortar interface

side, and Mg increases in the bentonite at the CB-interface. These anomalies are accompanied by the decreasing of Si and Al.

At the bentonite side, Mg concentration increased substantially in a length  $< 1000 \mu\text{m}$  from the CB-interface (from approximately 5 to  $>20$  at.% within the first  $50 \mu\text{m}$ ), but the increase of concentration from 6 to 18 months was short (Fig. 5a).

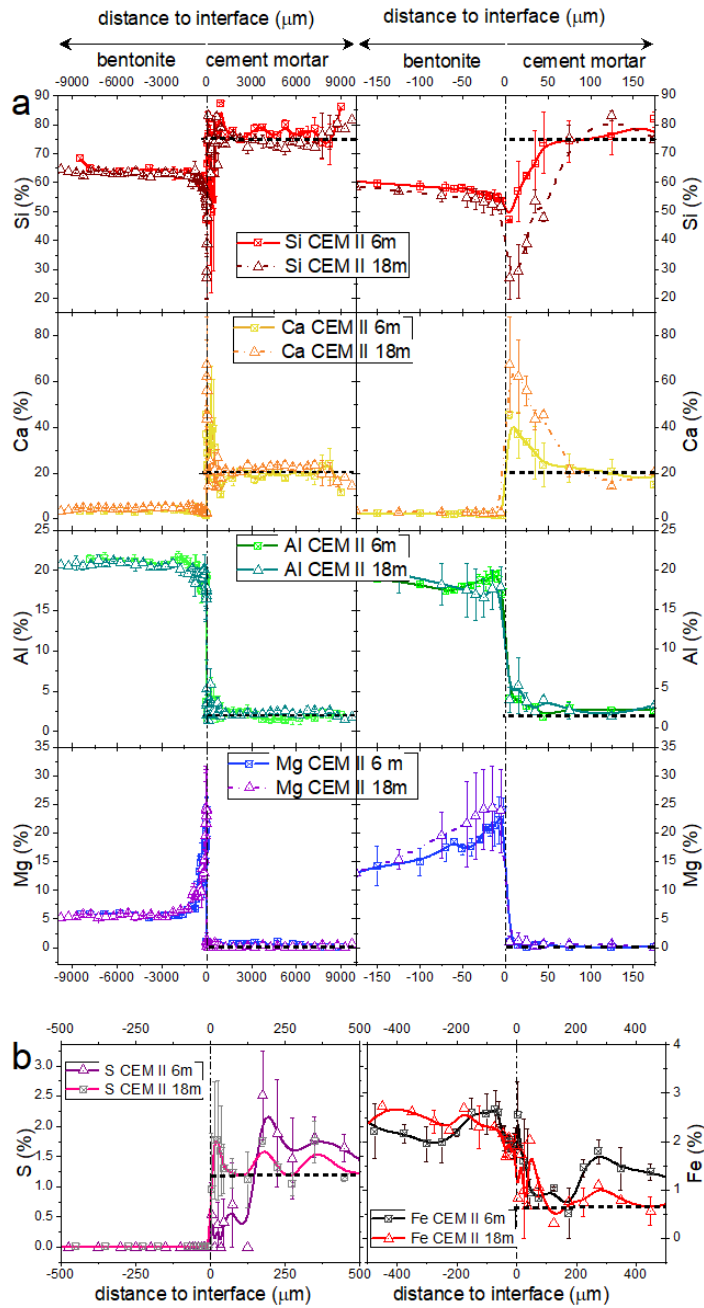




**Fig. 5.** Chemical profiles of composition in bentonite-CEM II cement mortar experiments after 6 and 18 months. All profiles were obtained based on the average values of the duplicated experiments and include error bars of standard deviation. Each profile is depicted at different ranges: from -9000 to 9000  $\mu\text{m}$  (left column) and from -200 to 200  $\mu\text{m}$  (right column) (a). The CB-interface (placed at 0  $\mu\text{m}$ , black dashed line) was taken as a reference. Additionally, a reference horizontal dotted line of the unaltered cement mortar reference sample is plotted for each element. Separately, the S and Fe profiles nearest to CB-interface (0-500  $\mu\text{m}$ ) are plotted at the bottom of figure (b).

Ca increases its relative concentration near the CB interface, in the cement mortar side. As for Mg, an increment of Ca concentration is observed from 6 to 18 month, but in this case, the increment is significant (20 at.% initially, 40% after 6 months and 60% after 18 months, as maximum averaged values). Therefore, the processes associated to the Ca enrichment does not seem to have reached a stationary state. Such a high increase is followed by a 1-2 mm Ca minimum, which is less pronounced after 18 months. This minimum agrees with the decalcification of C-S-H (lower Ca/Si ratios at the CB interface in Fig. 4a) and a presumably portlandite dissolution zone that causes calcite precipitation at the cement mortar side, as further confirmed by the GI-XRD study (section 4.3.1).

According to the possibility of C-A-S-H formation in the CB-interface, the Al profiles tend to increase with time in the first  $\mu\text{m}$  of the cement mortar side (<25  $\mu\text{m}$ ). Fig. 5b shows the profile evolution of S and Fe in a narrow -500 to 500  $\mu\text{m}$  band. S is depleted after 6 months but is relatively concentrated in the cement mortar side of the interface after 18 months. However, a certain amount of transfer of Fe from bentonite to cement matrix is evident with rather irregular distribution.

#### 4.1.3. SEM-EDX: surface interface crystal aggregate morphologies and composition

The nature of the Ca or Mg anomalies detected, mainly at the CB-interfaces and occasionally at the CW-interfaces (in the case of Ca), were first approached by exploration of singular crystal aggregates found in the fresh pristine surfaces separated at the end of the experiments. The composition of singular phases determined in the surface interfaces corresponding to B1, C1 and C3 slices and their distribution are indicated in Table 3. The characteristic morphologies of main phases and morphologies identified phases are illustrated by the SEM micrographs (Fig. 6).

Regarding to the bentonite interface, high Mg/Si platy (flat) and sheet (curled) like morphologies forming sometimes a Mg-rich crust were identified in B1 at any time (Fig. 6a and 6b). As for cement mortar side, the surface of the interface from C1 subsample was plenty of euhedral sphenoidal calcite microcrystals precipitation resulting in the formation of carbonated crusts (Fig. 6c, 6e, 6g). In addition, C-S-H, C-A-S-H, ettringite (6f, 6i and 6d, respectively) and hexagonal platy morphologies of C1-Aluminium Ferrite monosulfate phases (AFm), presumably Friedel salt-monosulfate AFm phases, (Fig. 6h) were observed. Mainly ettringite was found as the

main mineral phase, either in C1 (from the CB-interface) or C3 (from the CW-interface), and was significantly less frequent in the 18 months experiments at the CW-interface, indicating dissolution in this extreme.

**Table 3.** Summary of the observed phases and morphologies localized in slices B1-C1 (CB-interface surfaces) and C3 (CW-interface surfaces)

Experiment	Surface interface	High Mg-Si crust/matrix	Mg-Si rich platelets	*C-A-S-H	Calcite	**Ettringite	***AFm	****C-S-H
18-Exp1	B1	X			X(-)			
	C1			X	X			
	C3					X		
18-Exp2	B1	X	X		X(-)			
	C1		X	X	X	X	X	
	C3			X				
6-Exp1	B1	X			X			
	C1				X(+)	X(+)	X(+)	X(+)
	C3							
6-Exp2	B1	X	X(-)			X		
	C1			X		X	X	
	C3					X(+)	X	

\*C-A-S-H: Calcium aluminium silicate hydrate ( $Al/(Al+Si) = 0.2$ , and  $Ca/Si \sim 0.8$ ). \*\*Ettringite ( $Al/S = 0.7$ , and  $Ca/S = 2$ ). \*\*\*AFm: Calcium aluminium monosulphate ( $Al/S > 2$ ;  $Ca/S > 4$ ). \*\*\*\*C-S-H: Calcium silicate hydrate:  $Ca/Si = 0.6-2.3$ ). X, (+), (-) indicate "presence", "high presence", and "medium-low presence", respectively.

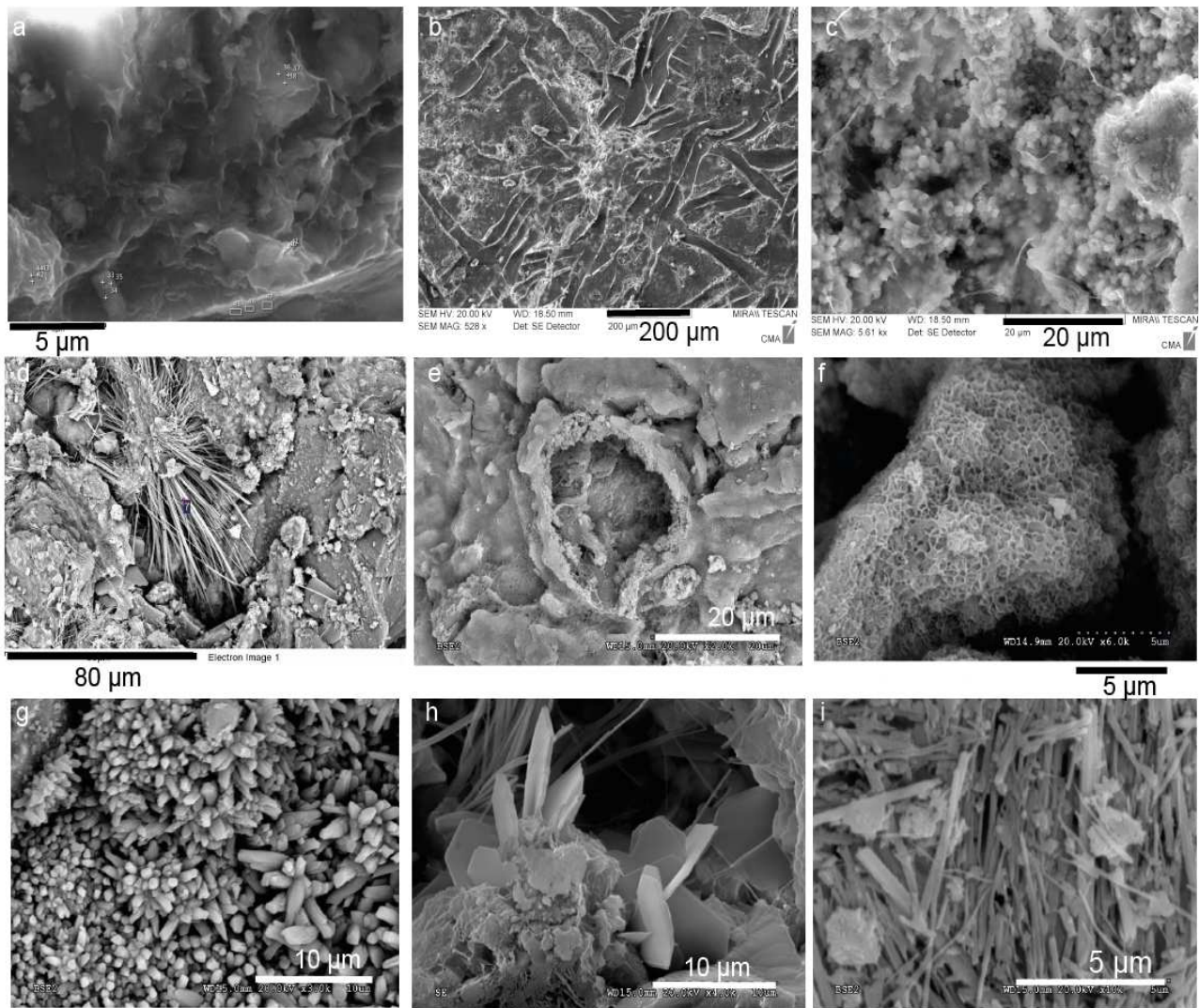


**Fig. 6.** SEM micrographs of the summary of phases and morphologies found in fresh pristine surface interfaces from B1-C1-C3 slices. (a) Mg-Si-rich platy morphologies. (b) Mg-Si-rich crust shaped by fibres of the PTFE membrane. (c) Calcite crystals growing among C-S-H. (d) Ettringite needles observed after 6 months in C1. (e) Calcite crust. (f) C-S-H. (g) Calcite sphenoidal crystal aggregates observed after 6 months. (h) Ca-Al-(S, Cl) crystals. (i) C-A-S-H needles. (Identification was made according to the chemical formula and the EDX).

## 4.2. X-ray diffraction on bentonite

### 4.2.1. GI-XRD 0.5° and $\theta$ -2 $\theta$ scans on bentonite

The GI-XRD analyses and  $\theta$ -2 $\theta$  scans under the GI-XRD configuration facilitated study of the mineralogy in the first 10  $\mu\text{m}$  of the surface interface of bentonite exposed to the influence of the CEM II-C porewater (Fig. 7a). The difference between GI-XRD 0.5° and  $\theta$ -2 $\theta$  used in this description is that the first is more superficial and the second corresponds to the diffracting result of higher sample volume.

The diffractograms at the interface of the reacted surface bentonite samples are characterized by the presence of 7.6-7.4 Å broad reflections not visible in the reference bentonite. These reflections were developed in all the  $\theta$ -2 $\theta$  scans, but they are not developed in the GI-XRD analyses performed on samples that reacted for 6 months. At lower angles, a critical intensity decline of the 14-15 Å reflection was observed, more generalized after 6 than after 18 months. In addition, a small shift is detected from 15.0 Å in the bentonite reference towards 14.8-14.5 Å in both sets of experiments (6 and 18 months). This shift is correlated with a small decrease in the position of the second-order basal reflection at 4.9-4.8 Å  $d$ -spacings, that becomes significantly more intense compared with the reference sample. These effects are better visualized by the  $\theta$ -2 $\theta$  scans in all experiments.

Characteristic di-octahedral Mnt reflections at 1.49 Å were found in the reference bentonite, and a broad band centred in 1.54-1.53 Å is always present in the reacted bentonite samples, indicating a tri-octahedral component that can be linked to the Mg/Si increase near the interface with the cement mortar. Quartz is occasionally present, as evidenced by a sharp reflection at 1.55 Å.

With respect to the more superficial GI-XRD 0.5° analysis, a broad reflection at 1.54-1.53 Å, observed after 18 months, is not present after 6 months neither the reference bentonite, which could be an indication of the precipitation of a tri-octahedral phase at long term. The 14-15 Å reflection, characteristic of the basal spacing of smectite is not present, indicating that the neogenic clay mineral presents high stacking disorder

at the surface.

It is important to note how the  $\theta$ -2 $\theta$  scans demonstrate the presence of the calcite 3.03 Å peak, which is not detectable in the reference sample, thus confirming that the carbonation is not homogeneously distributed at the first microns of the bentonite interfaces.

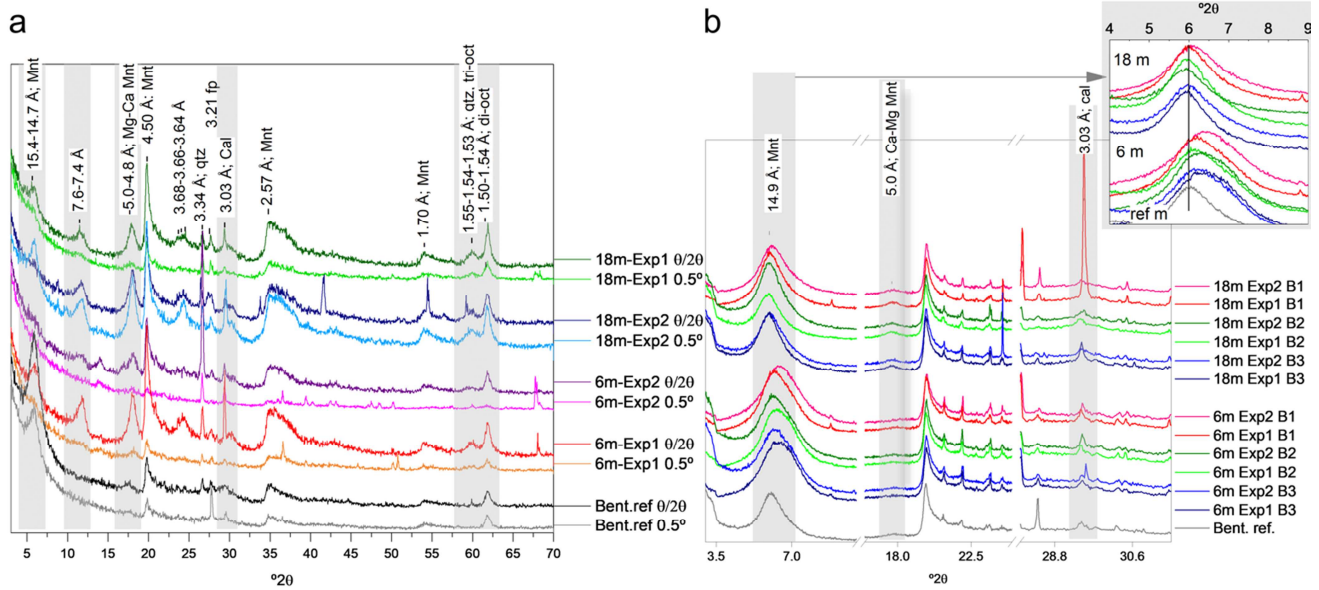


**Fig. 7** (a). GI-XRD analyses and  $\theta$ - $2\theta$  scans over flat fresh solid subsamples from the surface of bentonite. Numbers indicate d-values in Å; Mg-Ca Mnt: Mg-Ca montmorillonite, qtz: quartz, fp: feldspars, Cal: calcite, di: di-octahedral sheet, tri: tri-octahedral sheet. (b) XRD on randomly oriented powder bentonite samples at different distances from the interface (0-3 mm at B1; 3-6 mm at B2; 6-9 mm at B3) and different time scales (6 and 18 months). Upper right corner: close-up image of the (001) basal reflection region ( $4$ - $9^\circ$   $2\theta$ ). Bent. ref: diffractograms of the unaltered reference bentonite.

#### 4.2.2. Random powder X-ray diffraction on bentonite

The XRD analyses on powder samples supply information on the time evolution and spatial alteration of bentonite as a function of distance from the CB interface (Fig. 7b). Subtle variations were found in the (001)-reflection region ( $5$ - $8^\circ$   $2\theta$  position). Two shifts can be observed in that region related to the time evolution. First, the reference bentonite diffractogram shows reflections at  $\sim 15.0$  Å, and the diffractograms obtained after 6 months present these reflections at  $\sim 14.5$  Å, with a tail towards high angles compared with the 18 months experiments, where the basal reflection increases again to  $15$  Å and is more symmetrical. This differentiation in the basal space might be related to a change of the cations population in the interlayer. The initial Ca-Mg bentonite becomes slightly richer in monovalent cations ( $\text{Na}^+$ ,  $\text{K}^+$ ) as a result of local precipitation of Ca and Mg phases, however, the rate of transformation decreases with time and the population distribution is further homogenized as a result of the preferential leaching of monovalent cations out of the column (section 4.5).

In contrast to the small perturbations detected in Mnt by XRD on randomly oriented powder samples, the presence of the  $3.03$  Å reflection, characteristic of calcite, in one of the B1 slices run for 18 months (close to the cement mortar) is significant compared to all the other diffractograms. This observation is in agreement with the presumable calcite precipitation at both sides of the interface.



### 4.3. X-ray diffraction on cement mortar

#### 4.3.1. GI-XRD $0.5^\circ$ and $\theta$ - $2\theta$ scans on cement mortar

The main geochemical perturbations that can be remarked by XRD on the cement mortar are related to the evolution of ettringite, gypsum, portlandite and calcite mineral phases as they are well crystalline (Fig. 8a).

Distinctive reflections of gypsum and portlandite ( $7.6 \text{ \AA}$  and  $4.9 \text{ \AA}$ , respectively) were identified in the reference CEM II-C but are absent after 6 and 18 months.

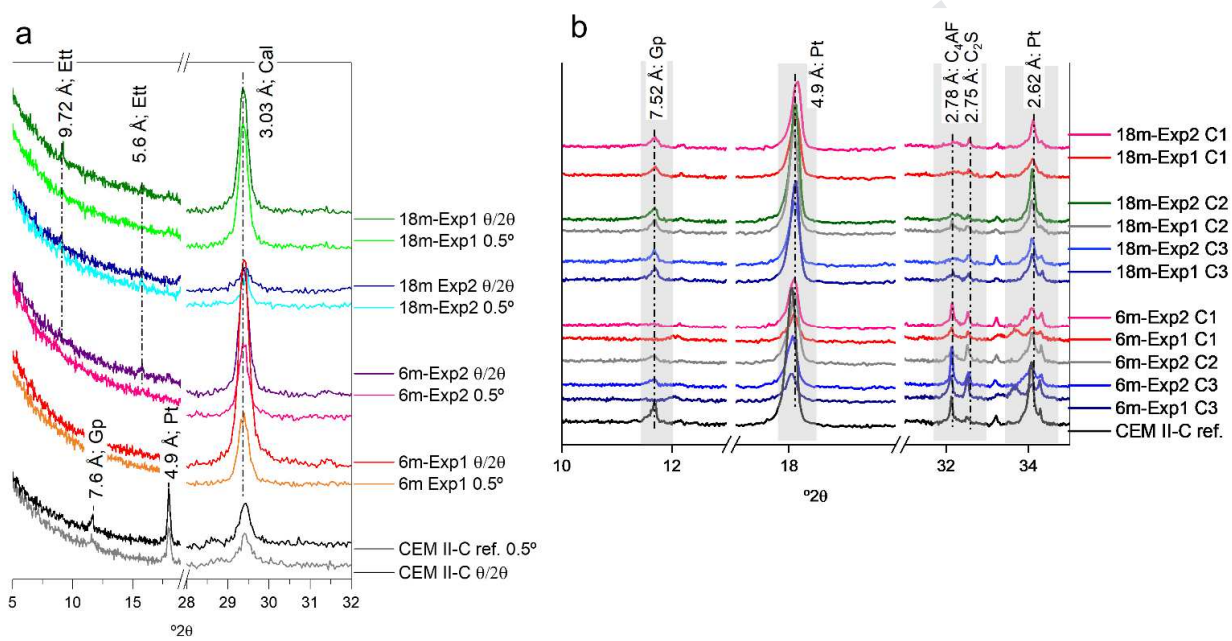


**Fig. 8.** (a) Close-up view of the  $\theta$ - $2\theta$  scans and GI-XRD analyses performed on the flat surface interface of CEM II-C. (b) Close-up view of the XRD patterns of cement mortar on randomly oriented powder samples at different distances from the interface (0-3 mm at C1; 3-6 mm at C2; 6-9 mm at C3) and at different time scales (6 and 18 months). Numbers indicate d-values in Å. Ett: ettringite, Cal: calcite, Gp: gypsum, Pt: portlandite, C<sub>4</sub>AF: calcium aluminoferrite, C<sub>2</sub>S: di-calcium silicate.

Characteristic reflections of ettringite ( $9.8 \text{ \AA}$  and  $5.6 \text{ \AA}$ ) were found after 6 and 18 months, but these reflections did not appear evident in the reference CEM II-C. Most of the ettringite found can be considered as secondary ettringite.

The reflections at  $3.03 \text{ \AA}$ ,  $3.86 \text{ \AA}$ ,  $1.91 \text{ \AA}$  and  $1.87 \text{ \AA}$ , characteristic of calcite, increase in intensity as time evolve. This is observed comparing the reference cement mortar with the altered cement mortars after 6 and 18 months, however, there is a substantial variation comparing the duplicated experiments. These variations indicate that the uneven distribution in calcite coatings might be better developed in macropores, as shown in Fig. 6g.



#### 4.3.2. Random powder X-ray diffraction on cement mortar

As observed for the bentonite slices, subtle differences were found in cement mortar by XRD on randomly oriented powder samples (Fig. 8b). A detailed study of the range between the 32 and 33 °2 $\theta$  positions shows an intensity decrease in the characteristic reflections of anhydrous phases, such as calcium aluminoferrite (C<sub>4</sub>AF) and di-calcium silicate (C<sub>2</sub>S) after 18 months (2.74 Å and 2.78 Å, respectively). These rearrangements occur as a result of progressive hydration of the anhydrous phases and the formation of secondary C-S-H characterized by a disordered structure and broad and weak diffraction maxima (Grangeon et al., 2013), which complicate their identification.

Minor differences were also found in the spatial progress by the study of samples C1, C2 and C3. The 6 and 18 months experiments showed a small decrease in the 7.56 Å reflection, characteristic of gypsum, and the reflections at 4.9 and 2.62 Å, characteristic of portlandite, suggesting their dissolution (Fig. 8b). However, the increase of calcite reflections, previously shown by the  $\theta$ -2 $\theta$  scans in the first  $\mu$ m of the surface interfaces, were not found across C1, C2 and C3 and, therefore, the carbonation process could occur only in a close spatial range at the immediate proximity to the interface with bentonite.

#### 4.4. Specific surface area

The SSA analyses performed throughout the bentonite and cement mortar slices to assess their spatial and temporal evolution are shown in Fig. 9. At the bentonite side, three main observations can be outlined: (i) the lower SSA values compared with the reference bentonite, (ii) the decrease in SSA from 6 to 18 months, and (iii) the decreasing tend of SSA away from the interface. At the CEM II-C side, C3 slices (facing the water interface) presents a slightly higher SSA than the reference sample. In addition, as time evolves from 6 to 18 months, the C2 and C1 slices increase in SSA.

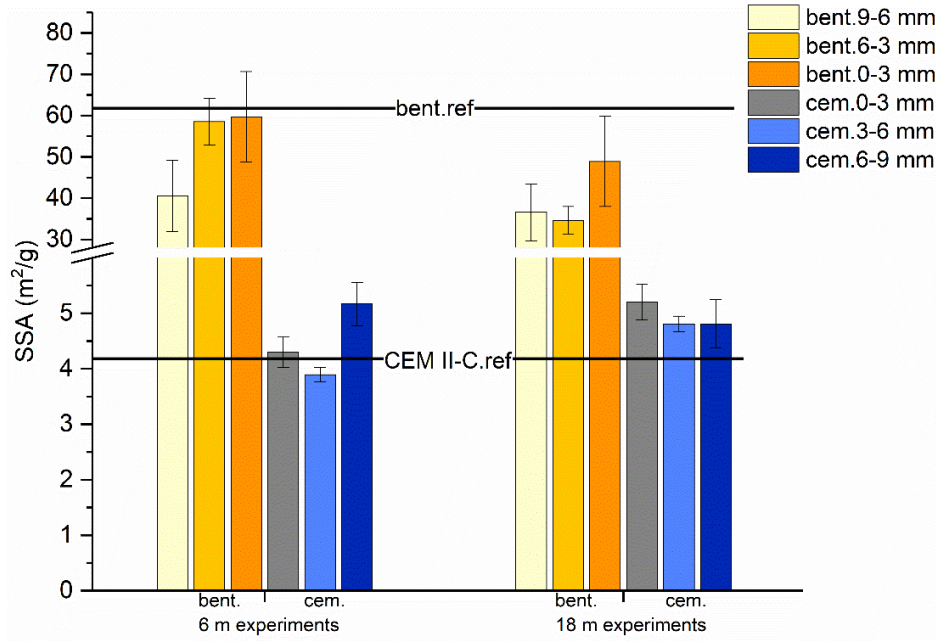


**Fig. 9.** SSA of bentonite and CEM II-C as a function of distance from the C-B interface. Note that the CB-interface is located between the orange and grey bars, and the CW-interface is located at the end of the dark blue bars.

#### 4.5. Effluent parameters

The hydraulic conductivity (H. C.) was calculated by the outflow data considering that the initial time corresponds to the beginning of the infiltration. The H. C. remains stable in the range  $10^{-12}$ - $10^{-13}$  m/s (Fig. 10a) for the whole experimental time (up to 18 months). In the averaged experiments performed for 6 months the H. C. is higher than in the experiments performed for 18 months, but this should only be attributed to random differences derived from the preparation of the initial materials that are not completely homogeneous. The accumulated volume of effluent collected in one of the experiments run for 6 months was similar to those collected in the experiments run for 18 months, indicating the presence of preferential pathways for fluid circulation in that specific experiment. As the data are presented as averaged values for experiments performed for 6 and for 18 months, the error bars for the 6 months experiments in Fig. 10a are large.

Bentonite is compacted at its characteristic water content (approximately 14 wt.%) in its dried state at the laboratory ambient conditions (30 – 50 % R. H.). Therefore, the initial conditions are unsaturated. Aqueous  $\text{SO}_4^{2-}$ ,  $\text{Cl}^-$ ,  $\text{Na}^+$  and  $\text{K}^+$  are leached initially in higher concentrations than all other ions and correspond with the displaced bentonite porewater (Fig. 10b), known to be concentrated in these ions (Cuevas et al., 2002).  $\text{SO}_4^{2-}$  is almost exhausted after 7-8 pore volumes (one pore volume is calculated as the total porosity of bentonite,  $\sim 1.3 \text{ cm}^3$ ),

whereas  $\text{Cl}^-$  decreases drastically its concentration at the beginning and gets mostly exhausted after 13-14 pore volumes.  $\text{Na}^+$  is the dominant cation and achieves a low constant value after 6 – 10 pore volumes, presumably regulated by the cation exchange equilibrium ruled by Mnt, since  $\text{Na}^+$  is the less selective cation in the cation exchange equilibrium concerning the FEBEX bentonite (Fernández et al., 2004). The alkalinity, represented mainly by  $\text{HCO}_3^-$  (with certain contribution of  $\text{CO}_3^{2-}$ , not accounted in the charge balance), becomes the main anion with time (after 6 pore volumes). The  $\text{Ca}^{2+}$  concentration critically decreases to 21-23 mg/L, and aqueous  $\text{Mg}^{2+}$  becomes negligible in solution due to fixation related to the Mg increase in the solid phase determined at the bentonite interface with cement mortar (section 4.1.2).

The pH and aqueous silica remained almost constant regardless of time (Table 4). These values are near the characteristics of FEBEX-bentonite porewater: 10 – 30 mg/L  $\text{SiO}_2$  (cristobalite dissolution, Williams et al., 1985), pH = 9 – 7, depending on leaching or squeezing method used, respectively (Fernández et al., 2004). In spite of these authors, who used edge site protonation constants to explain the FEBEX bentonite pH buffering, Cuevas et al. (2006) calculated that the characteristic pH is obtained by taking into account the coupled reaction of cation exchange and calcite dissolution present in bentonite:  $\text{CaCO}_3 + \text{H}^+ + 2 \text{NaX} \rightleftharpoons \text{HCO}_3^- + \text{CaX}_2 + 2 \text{Na}^+$ .

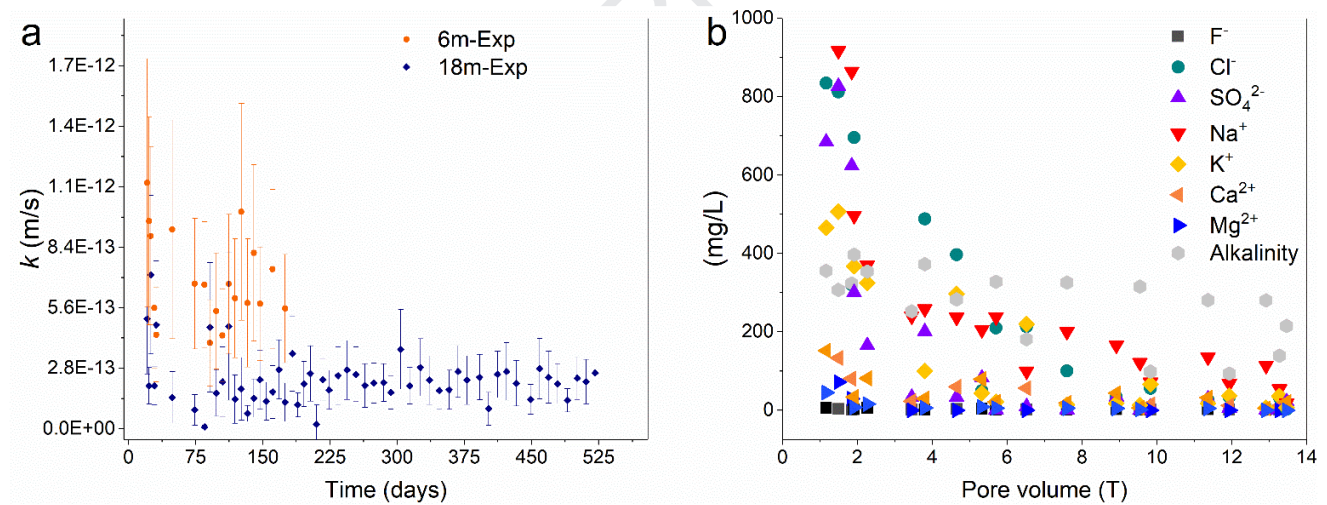


**Fig. 10.** (a) Averaged hydraulic conductivity calculated as a function of time for experiments performed for 6 (orange) and 18 months (blue). (b) Concentrations of major ions collected at the end of the bentonite side; data for experiments conducted for 6 and 18 months are represented in the same plot.

**Table 4.** pH and aqueous silica results after 6 and 18 months.

Experiment	pH	$\text{SiO}_{2(\text{aq})}$ (mg/L).
6m-Exp	$8.2 \pm 0.1$	$12.8 \pm 0.1$
18m-Exp	$8.3 \pm 0.1$	$17.3 \pm 0.2$

6m-Exp: experiments conducted for 6 months, 18m-Exp: experiments conducted for 18 months.

## 5 Discussion

### 5.1 Mg perturbation

The results of small-scale laboratory experiments reveal the development of Mg perturbation in the cement mortar/FEBEX-bentonite interface at a notably shorter time compared with the FEBEX *in situ* experiment performed at large scale. Indeed, limited development of this perturbation is observed in the laboratory experiments from 6 to 18 months. Large accumulation of Mg was identified in the FEBEX *in situ* experiment after 13 years of concrete-bentonite interaction in highly similar conditions but at much larger spatial scale (Fernández et al., 2017). 10 m<sup>3</sup> of concrete in contact with 40 m<sup>3</sup> of FEBEX-bentonite were placed in the *in situ* experiment, while 0.57 cm<sup>3</sup> of cement mortar and 0.57 cm<sup>3</sup> of FEBEX-bentonite were placed in the laboratory experiment. The Mg perturbation reached an extension of 2-3 mm from the CB-interface in the FEBEX *in situ* experiment, whereas a length < 1 mm was observed in this work. The magnitude of the Mg perturbation in the FEBEX *in situ* experiments, that reached up to 20-45 wt.% in bentonite at the interface (Fernández et al., 2017) cannot be directly compared with the results obtained in the present study (~25 at.%) because of the different units of measurement. However, a simple estimation reveals similar degree of Mg enrichment in the accumulation zone near the interface.

The Mg increase has not only been observed in cement or concrete/bentonite interfaces. Stiff clay rocks under the influence of high-pH concrete pore water (pH > 12) showed a characteristic Mg perturbation (e.g. Mäder et al., 2017; Moyce et al., 2014). In concrete/clay systems, this perturbation is also evidenced at the concrete side and it is remarkable when low-pH cementitious materials have been tested (Dauzères et al., 2016).

Mg-silicates can precipitate as a result of the alkaline influence supplied by the cement. The nature of the Mg-silicates formed in large scale experiments, such as the FEBEX *in situ* experiment, is complex considering the variety of compositions that have been identified as a result of the bentonite alkaline alteration. In a similar way as Al may be accommodated in C-S-H phases to form C-A-S-H, exchangeable Mg can also be incorporated in silicates to form saponite-like smectites, as predicted by Roosz et al. (2015) or used to form a variety of Mg-silicates, including M-S-H phases (e.g. Fernández et al., 2018).

The variety of Mg-silicates identified in literature as a result of cement/clay interaction are compatible with the presence of tri-octahedral phyllosilicates 1:1 or 2:1 sheet silicate (Shimbashi et al., 2018). The complex chemical compositions of the zone with anomalous high Mg concentrations have been found to be compatible with a

mixture of brucite and Mnt, as the Al content maintained constant, and the di-octahedral character of the Mnt remained, as observed by the XRD-diffraction patterns (Cuevas et al., 2018b; Fernández et al., 2017). In fact, Lerouge et al. (2017) identified grain compositions related to Mg perturbation that were highly rich in Mg and compatible with these types of mixtures. In the present experiments, structural characterization of the bentonite interface surface reveals a broad peak at 7.5 Å, that can be related to mixture such as an intercalated  $\text{Mg}(\text{OH})_2$ -Mnt complex. This mixture was considered as one of the main reaction components of the early stage hyperalkaline alteration of Mg-Mnt in presence of KOH 0.5 M solutions (Fernández et al., 2013). The generalized presence of this type of phase in these early surface experiments can point to these types of phases as a precursor of more common mineral phases formed in Mg-rich natural alkaline environments as saponite or stevensitic minerals (Eberl et al., 1982). These Mg neogenic phases reveal structural properties similar to those of 2:1 and 1:1 sheet silicates and generally form a poorly crystalline but precise structure that is still under investigation (Walling and Provis, 2016). As in this work, M-S-H has been described as a homogeneous gel-like structure with a sheet-like morphology and Mg/Si ratios greater than 0.8 (Bernard et al., 2017; Bernard et al., 2019; Lothenbach et al., 2015), but their formation has been primarily reported in the concrete side. The presence of any Mg-silicate hydrated phase in bentonite is highly difficult to ascertain because of mixing with other complex clay mineral phases with significant Al quantities.

## 5.2 Ca perturbation

At the cement mortar side, the formation of a calcite skin ( $\sim 50 \mu\text{m}$  from the CB-interface) was identified after 6 months and more pronounced after 18 months. This Ca increase, associated with the precipitation of soluble inorganic carbon species, occurs coupled to the decalcification of the C-S-H, identified by SEM-EDX analyses on the cement and by the profiles of chemical composition.  $\text{HCO}_3^-$ , that becomes the dominant aqueous anion species after 6 months, may act as a source of carbonates precipitation at high pH, which indeed, is supported by the dissolution of portlandite.

The formation of calcite at the concrete-bentonite interface was also reported in the FEBEX *in situ* experiment as a result of interaction of  $\text{HCO}_3^-$  from the clay porewater and  $\text{Ca}^{2+}$  from concrete (Fernández et al., 2017), resulting in calcite precipitation that forms a protective crust of low porosity, that increases its resistance against groundwater and porewater penetration (Jenni et al., 2014). Therefore, the localized development of Ca increase, in the order of  $\mu\text{m}$  in cement mortar observed in the present study, evolves to the mm scale ( $\sim 1 \text{ mm}$ ) after 13 years of ageing in the FEBEX *in situ* experiment.

At the bentonite side, the Ca increase observed by the SEM-EDX profiles of chemical composition was not as significant as in the cement mortar side, although higher amounts of calcite than those naturally present in the

reference bentonite were detected by XRD. The Ca increase can be estimated as 1-5 at.% in the bentonite side, which is far from the Ca increase of 29-80 at.% detected at the cement mortar interface. It has been observed a certain amount of calcite dissolution affecting several cm to the concrete interface in certain locations in the FEBEX *in situ* experiments. Precipitation of calcite at the interface was also found in both, the bentonite and concrete sides, an effect that was clearly separated in the Mg-silicate precipitation. (Turrero and Cloet, 2017).

### 5.3 Al-S phase dynamics

Ettringite was almost always present in the studied cement mortar interface. SEM-EDX and XRD data suggest its formation as a secondary phase within the interface. Ettringite was not detected by XRD in the reference cement mortar sample or was less often observed, presenting different morphologies. The presence of ettringite is favoured by the limestone additions, since cement materials with higher quantities of carbonate additions tend to avoid the conversion of ettringite to AFm (Lothenbach et al., 2008). The origin of secondary ettringite comes from the incorporation of (i) Al supplied by Mnt dissolution (Gaucher and Blanc, 2006), (ii) S released by dissolution of gypsum and supplied by the porewater from bentonite, and (iii) Ca delivered by decalcification of C-S-H and portlandite present in the cement mortar (Cuevas et al., 2016). At long-term, ettringite is not stable at the interface. In the FEBEX *in situ* experiment, ettringite was detected within the concrete matrix but further from the interface and as secondary phase-filling pores (Alonso et al., 2017).

AFm phases seem to have been occasionally stabilized by incorporating  $\text{Cl}^-$  diffusing as a soluble species in bentonite porewater. Friedel salt is a more stable  $\text{Cl}^-$ -AFm phase and has also been described in the FEBEX *in situ* experiment further from the interface (Alonso et al., 2017).  $\text{Cl}^-$  monitoring is important because it is a potential corrosion agent of reinforced concrete (Chen and Mahadevan, 2008), but in this context, its role is of little relevance because  $\text{Cl}^-$  has a high diffusion rate, and  $\text{Cl}^-$  fixation by the cement AFm phases was not significant, as demonstrated by the  $\text{Cl}^-$  performance in the present experiment, that was easily leachable.

Al can also follow other reaction pathways, rather than forming Al-S ettringite phases. Ettringite coexists with carbonates, and C-A-S-H forms as a result of the Al supplied by bentonite pore fluids, as suggested by the SEM-EDX profiles of chemical composition (Section 4.1.2). The ability to accommodate cations from the pore fluid is inversely related to the Ca content of C-S-H, and after the observed decalcification process, C-S-H with lower Ca/Si ratios could easily uptake Al to form C-A-S-H phases (Fernández et al., 2016).



#### 5.4 Specific surface area

The SSA represents the external surface area exposed to the porous space, considering the edge sites (Fernández et al., 2013) and excluding the surface area of the internal basal planes. This parameter depends on sample pretreatment, exchangeable cations and microporosity (Kaufhold et al., 2010).

At the bentonite side, the SSA reduction in the samples compared with the reference bentonite could be related with the existence of certain clogging processes, presumably due to calcite or other nanoscale cements. This process promotes the aggregation of clay particles, thus hindering  $N_2(g)$  access to occluded pores, and consequently, the SSA decreases. With respect to the spatial evolution studied from the interface to the bentonite end, the increasing trend of the SSA nearest the CB-interface can be attributed to the decrease in the average size of the smectite particles affected by neogenic Mg-clay mineral nanocrystal aggregates. This newly formed phase can occupy larger pores, thus increasing the weight of the microporosity in the original pore distribution. We consider this interpretation to be more reliable than the increment of the microporosity due to a decrease in the major exchangeable cations of  $Ca^{2+}$  and  $Mg^{2+}$  (Metz et al., 2005) or the dissolution of Mnt and the consequent reduction of the 2:1 layers (Lowell and Shields, 2013). In our case, only a weak reflection displacement towards lower d-spacings in the basal reflection (001) was observed.

At the cement mortar side, the higher SSA found after 6 and 18 months at the CB and CW-interfaces compared with the intermediate sample (3-6 mm) and the reference cement mortar is attributed to the decalcification and formation of low Ca/Si C-S-H of lower crystal size and greater disorder, thus increasing the SSA (Phung et al., 2016).

#### 5.5 Evaluation of leachate

If the general SSA decrease observed in bentonite were attributed to precipitation of nanoscale cements and formation of Mg-Clays near the interface, as evidenced after 6 months, it could be related to the lower hydraulic conductivity values (Alonso et al., 2017) stabilized after < 6 months. (section 4.5). However, this observation does not agree with the increase in SSA from 6 to 18 months in the cement mortar side. This difference in behaviour can be explained because the leachate was collected at the end of the bentonite side, which control the fluid flow due to its low effective porosity and hydraulic conductivity. In the same way, the pH and silica results were similar to those characteristics of the reference FEBEX-bentonite. Therefore, the buffer characteristic of bentonite is demonstrated.

The high concentrations of sulphate and chloride found in the first pore volumes and the subsequent absolute decline mostly occur as a result of their depletion from the porewater of bentonite.  $Na^+$  is naturally present as 1/3

of the exchangeable cation complex in FEBEX-bentonite, but a subset of the  $\text{Na}^+$  and  $\text{K}^+$  might originate from the alkalis of the cement mortar, increasing their concentration at an early leaching stage. Later, the monovalent ions, together with  $\text{Ca}^{2+}$  and  $\text{Mg}^{2+}$ , suffer a decrease related to their regulation as exchangeable cations (mainly  $\text{Ca}^{2+}$ ,  $\text{Na}^+$ ) and the precipitation of calcite and Mg-silicates ( $\text{Mg}^{2+}$ ). The decrease in these exchangeable cations has also been described nearest the interface (Mäder et al., 2017) related to the precipitation of Mg-silicates.

## 6 Conclusions

This study assesses the geochemical reactions occurring at the early stage (0.5-1.5 years) of the interaction between cement mortar-CEM II and FEBEX-bentonite with the aim to facilitate a better comprehension of the large-spatial and long-term results observed after 13 years of concrete-bentonite interaction from the dismantling of the FEBEX *in situ* experiment. The expected reaction paths, which are more progressed in long-term experiments, are consistent with the initial evolution of the results summarized in this study:

Decalcification of C-S-H in an environment in which portlandite dissolution occurs and anhydrous phases are progressive hydrated.

Development of a Ca-carbonation skin (calcite) in the cement mortar side and dispersed precipitation of calcite in localized zones of bentonite.

Initial development of a Mg-perturbation at the bentonite side, related to the formation of precursors of Mg-clay 2:1 sheet silicates as the main neogenic phases expected at the long-term.

Formation of secondary ettringite at the cement mortar interface

The geochemical reactions observed at small spatial scale ( $\mu\text{m}$ ) and short-term (up to 18 months) are promising for development of reaction concepts and support modelling in the future, thus offering a useful prospective to advance upscaling of the concrete-bentonite interface perturbations at long-term.

## 7 Acknowledgements

This work was supported by funding from the European Union's Horizon 2020 Research and Training programme from EUROATOM [H2020-NFRP 2014, 2015] under grant agreement n°662147; CEBAMA. The authors thank Juan D. Rodriguez-Blanco Professor in Nanomineralogy from Trinity College Dublin for assistance with analytical support.

## 8 Supplementary material

A mathematical fitting of the chemical evolution of the outflow solution as a function of the pore volume is given in Tables S1 and S2.

## References

- Alonso, M.C., García Calvo, J.L., Cuevas, J., Turrero, M.J., Fernández, R., Torres, E., Ruiz, A.I., 2017. Interaction processes at the concrete-bentonite interface after 13 years of FEBEX-Plug operation. Part I: Concrete alteration. *Physics and Chemistry of the Earth, Parts A/B/C* 99, 38. <https://doi.org/10.1016/j.pce.2017.03.008>
- Bernard, E., Lothenbach, B., Chlique, C., Wyrzykowski, M., Dauzères, A., Pochard, I., Cau-Dit-Coumes, C., 2019. Characterization of magnesium silicate hydrate (M-S-H). *Cement and Concrete Research*, 116, 309. <https://doi.org/10.1016/j.cemconres.2018.09.007>
- Bernard, E., Lothenbach, B., Rentsch, D., Pochard, I., Dauzères, A., 2017. Formation of magnesium silicate hydrates (M-S-H). *Physics and Chemistry of the Earth, Parts A/B/C* 99, 142. <https://doi.org/10.1016/j.pce.2017.02.005>
- Berner, U., 1992. Evolution of pore water chemistry during degradation of cement in a radioactive waste repository environment. *Waste management* 12, 201. [https://doi.org/10.1016/0956-053X\(92\)90049-O](https://doi.org/10.1016/0956-053X(92)90049-O)
- Berner, U., Kulik, D.A., Kosakowski, G., 2013. Geochemical impact of a low-pH cement liner on the near field of a repository for spent fuel and high-level radioactive waste. *Physics and Chemistry of the Earth, Parts A/B/C* 64, 46. <https://doi.org/10.1016/j.pce.2013.03.007>
- Caballero, E., Jiménez de Cisneros, C., Huertas, F.J., Huertas, F., Pozzuoli, A., Linares, J., 2005. Bentonites from Cabo de Gata, Almería, Spain: a mineralogical and geochemical overview. *Clay Minerals* 40, 463. <https://doi.org/10.1180/0009855054040184>
- Chen, D., Mahadevan, S., 2008. Chloride-induced reinforcement corrosion and concrete cracking simulation. *Cement and Concrete Composites* 30, 227. <https://doi.org/10.1016/j.cemconcomp.2006.10.007>
- Churakov, S.V., Prasianakis, N.I.J.A.J.o.S., 2018. Review of the current status and challenges for a holistic process-based description of mass transport and mineral reactivity in porous media. *American Journal of Science* 318, 921. <https://doi.org/10.2475/09.2018.03>
- Cuevas, J., Ruiz, A. I., Fernández, R., 2018a. Investigating the Potential Barrier Function of Nanostructured Materials Formed in Engineered Barrier Systems (EBS) Designed for Nuclear Waste Isolation. *The Chemical Record*, 18, 7-8, 1065-1075. <https://doi.org/10.1002/tcr.201700094>
- Cuevas, J., Ruiz, A., Fernández, R., González-Santamaría, D., Angulo, M., Ortega, A., Torres, E., Turrero, M., 2018b. Authigenic Clay Minerals from Interface Reactions of Concrete-Clay Engineered Barriers: A New Perspective on Mg-Clays Formation in Alkaline Environments. *Minerals* 8, 362. <https://doi.org/10.3390/min8090362>
- Cuevas, J., Ruiz, A.I., Fernández, R., Torres, E., Escribano, A., Regadío, M., Turrero, M.J., 2016. Lime mortar-compacted bentonite–magnetite interfaces: An experimental study focused on the understanding of the

- EBS long-term performance for high-level nuclear waste isolation DGR concept. *Applied Clay Science* 124-125, 79. <https://doi.org/10.1016/j.clay.2016.01.043>
- Cuevas, J., Vigil de la Villa, R., Ramírez, S., Sánchez, L., Fernández, R., Leguey, S., 2006. The alkaline reaction of FEBEX bentonite: a contribution to the study of the performance of bentonite/concrete engineered barrier systems. *Journal of Iberian Geology* 32, 151-174
- Cuevas, J., Villar, M. V., Martín, M., Cobeña, J. C., Leguey, S., 2002. Thermo-hydraulic gradients on bentonite: distribution of soluble salts, microstructure and modification of the hydraulic and mechanical behaviour. *Applied Clay Science*, 22, 25-38. [https://doi.org/10.1016/S0169-1317\(02\)00109-6](https://doi.org/10.1016/S0169-1317(02)00109-6)
- Dauzères, A., Achiedo, G., Nied, D., Bernard, E., Alahache, S., Lothenbach, B., 2016. Magnesium perturbation in low-pH concretes placed in clayey environment—solid characterizations and modeling. *Cement and Concrete Research* 79, 137. <https://doi.org/10.1016/j.cemconres.2015.09.002>
- Dauzères, A., Le Bescop, P., Sardini, P., Cau Dit Coumes, C., 2010. Physico-chemical investigation of clayey/cement-based materials interaction in the context of geological waste disposal: Experimental approach and results. *Cement and Concrete Research*, 40, 8, 1327-1340. <https://doi.org/10.1016/j.cemconres.2010.03.015>
- Eberl, D.D., Jones, B.F., Khoury, H.N., 1982. Mixed-Layer Kerolite/Sstevensite from the Amargosa Desert, Nevada. *Clay and Clays Minerals* <https://doi.org/10.1346/CCMN.1982.0300501>.
- Ewing, R.C., Whittleston, R.A., Yardley, B.W.J.E., 2016. Geological disposal of nuclear waste: a primer. *Elements* 12, 233. <https://doi.org/10.2113/gselements.12.4.233>
- Fernández, A. M., Baeyens, B., Bradbury, M., Rivas, P., 2004. Analysis of the porewater chemical composition of a Spanish compacted bentonite used in an engineered barrier. *Physics and Chemistry of the Earth*, 29, 105-118. <https://doi.org/10.1016/j.pce.2003.12.001>
- Fernández, A. M., Kaufhold, S., Sánchez-Ledesma, D. M., Rey, J. J., Melón, A., Robredo, L. M., Fernández, S., Labajo, M. A., Clavero, M. A., 2018. Evolution of the THC conditions in the FEBEX in situ test after 18 years of experiment: Smectite crystallochemical modifications after interactions of the bentonite with a C-steel heater at 100 °C. *Applied Geochemistry*, 98, 152-171. <https://doi.org/10.1016/j.apgeochem.2018.09.008>
- Fernández, R., González-Santamaría, D., Angulo, M., Torres, E., Ruiz, A. I., Turrero, M. J., Cuevas, J. 2018. Geochemical conditions for the formation of Mg silicates phases in bentonite and implications for radioactive waste disposal. *Applied Geochemistry* 93, 1. <https://doi.org/10.1016/j.apgeochem.2018.03.012>
- Fernández, R., Ruiz, A.I., Cuevas, J., 2016. Formation of CASH phases from the interaction between concrete or cement and bentonite. *Clay Minerals* 51, 223. <https://doi.org/10.1180/claymin.2016.051.2.09>
- Fernández, R., Torres, E., Ruiz, A.I., Cuevas, J., Alonso, M.C., García Calvo, J.L., Rodríguez, E., Turrero, M.J., 2017. Interaction processes at the concrete-bentonite interface after 13 years of FEBEX-Plug operation. Part II: Bentonite contact. *Physics and Chemistry of the Earth, Parts A/B/C* 99, 49. <https://doi.org/10.1016/j.pce.2017.01.009>
- Fernández, R., Vigil de la Villa, R., Ruiz, A.I., García, R., Cuevas, J., 2013. Precipitation of chlorite-like structures during OPC porewater diffusion through compacted bentonite at 90°C. *Applied Clay Science* 83-84, 357. <https://doi.org/10.1016/j.clay.2013.07.021>

- García Calvo, J.L., 2012. Desarrollo de materiales de construcción con cemento de bajo pH, compatibles con la barrera de ingeniería de un almacenamiento geológico profundo de residuos radiactivos de alta actividad. Universidad Autónoma de Madrid, Madrid, Spain. <http://hdl.handle.net/10486/12309>
- García Calvo, J.L., Hidalgo, A., Alonso, C., Fernández Luco, L., 2010. Development of low-pH cementitious materials for HLRW repositories: Resistance against ground waters aggression. *Cement and Concrete Research* 40, 1290. <https://doi.org/10.1016/j.cemconres.2009.11.008>
- Garraón, A., Gómez, P., Turrero, M.J., Torres, E., Buil, B., Sánchez, L., Peña, J., 2017. Hydrogeochemical characterisation of the groundwater in the FEBEX gallery. NAGRA Technical Report NAB 16-14, 125 pp.
- Gaucher, E.C., Blanc, P., 2006. Cement/clay interactions—a review: experiments, natural analogues, and modeling. *Waste Management* 26, 776. <https://doi.org/10.1016/j.wasman.2006.01.027>
- González-Santamaría, D., Angulo, M., Ruiz, A., Fernández, R., Ortega, A., Cuevas, J., 2018. Low-pH cement mortar-bentonite perturbations in a small-scale pilot laboratory experiment. *Clay Minerals* 53, 237. <https://doi.org/10.1180/clm.2018.16>
- Grangeon, S., Claret, F., Linard, Y., Chiaberge, C., 2013. X-ray diffraction: a powerful tool to probe and understand the structure of nanocrystalline calcium silicate hydrates. *Acta crystallographica Section B, Structural science, crystal engineering and materials* 69, 465. <https://doi.org/10.1107/S2052519213021155>
- Jenni, A., Mäder, U., Lerouge, C., Gaboreau, S., Schwyn, B., 2014. In situ interaction between different concretes and Opalinus Clay. *Physics and Chemistry of the Earth, Parts A/B/C* 70-71, 71. <https://doi.org/10.1016/j.pce.2013.11.004>
- Kaufhold, S., Dohrmann, R., Klinkenberg, M., Siegesmund, S., Ufer, K.J., 2010. N<sub>2</sub>-BET specific surface area of bentonites. *Journal of colloid interface science* 349, 275. <https://doi.org/10.1016/j.jcis.2010.05.018>
- Khoury, H.N., Salameh, E., Abdul-Jaber, Q., 1985. Characteristics of an unusual highly alkaline water from the Maqarin area, northern Jordan. *Journal of Hydrology* 81, 79. [https://doi.org/10.1016/0022-1694\(85\)90168-4](https://doi.org/10.1016/0022-1694(85)90168-4)
- Lerouge, C., Gaboreau, S., Grangeon, S., Claret, F., Warmont, F., Jenni, A., Cloet, V., Mäder, U., 2017. In situ interactions between Opalinus Clay and Low Alkali Concrete. *Physics and Chemistry of the Earth, Parts A/B/C* 99, 3. <https://doi.org/10.1016/j.pce.2017.01.005>
- Lothenbach, B., Le Saout, G., Gallucci, E., Scrivener, K., 2008. Influence of limestone on the hydration of Portland cements. *Cement and Concrete Research* 38, 848. <https://doi.org/10.1016/j.cemconres.2008.01.002>
- Lothenbach, B., Nied, D., L'Hôpital, E., Achiedo, G., Dauzères, A., 2015. Magnesium and calcium silicate hydrates. *Cement and Concrete Research* 77, 60. <https://doi.org/10.1016/j.cemconres.2015.06.007>
- Lowell, S., Shields, J.E., 2013. Powder surface area and porosity. Springer Science & Business Media
- Mäder, U., Jenni, A., Lerouge, C., Gaboreau, S., Miyoshi, S., Kimura, Y., Cloet, V., Fukaya, M., Claret, F., Otake, T., Shibata, M., Lothenbach, B., 2017. 5-year chemico-physical evolution of concrete–claystone interfaces, Mont Terri rock laboratory (Switzerland). *Swiss Journal of Geosciences* 110, 307. <https://doi.org/10.1007/s00015-016-0240-5>

- Metz, V., Raanan, H., Pieper, H., Bosbach, D., Ganor, J., 2005. Towards the establishment of a reliable proxy for the reactive surface area of smectite. *Geochimica et Cosmochimica Acta* 69, 2581. <https://doi.org/10.1016/j.gca.2004.11.009>
- Moyce, E.B.A., Rochelle, C., Morris, K., Milodowski, A.E., Chen, X., Thornton, S., Small, J.S., Shaw, S., 2014. Rock alteration in alkaline cement waters over 15 years and its relevance to the geological disposal of nuclear waste. *Applied Geochemistry* 50, 91. <https://doi.org/10.1016/j.apgeochem.2014.08.003>
- Phung, Q.T., Maes, N., Jacques, D., De Schutter, G., Ye, G., 2016. Investigation of the changes in microstructure and transport properties of leached cement pastes accounting for mix composition. *Cement and Concrete Research* 79, 217. <https://doi.org/10.1016/j.cemconres.2015.09.017>
- Roosz, C., Grangeon, S., Blanc, P., Montouillout, V., Lothenbach, B., Henocq, P., Giffaut, E., Vieillard, P., Gaboreau, S., 2015. Crystal structure of magnesium silicate hydrates (M-S-H): The relation with 2:1 Mg–Si phyllosilicates. *Cement and Concrete Research* 73, 228. <https://doi.org/10.1016/j.cemconres.2015.03.014>
- Savage, D., Walker, C., Arthur, R., Rochelle, C., Oda, C., Takase, H., 2007. Alteration of bentonite by hyperalkaline fluids: A review of the role of secondary minerals. *Physics and Chemistry of the Earth, Parts A/B/C*, 32, 1-7, 287-297. <https://doi.org/10.1016/j.pce.2005.08.048>
- Savage, D., 2011. A review of analogues of alkaline alteration with regard to long-term barrier performance. *Mineralogical Magazine*, 75, 4, 2401-2418. <https://doi.org/10.1180/minmag.2011.075.4.2401>
- Shimbashi, M., Sato, T., Yamakawa, M., Fujii, N., Otake, T., 2018. Formation of Fe- and Mg-Rich Smectite under Hyperalkaline Conditions at Narra in Palawan, the Philippines. *Minerals* 8, 155. <https://doi.org/10.3390/min8040155>
- Techer, I., Bartier, D., Boulvais, P., Tinseau, E., Suchorski, K., Cabrera, J., Dauzères, A., 2012. Tracing interactions between natural argillites and hyper-alkaline fluids from engineered cement paste and concrete: Chemical and isotopic monitoring of a 15-years old deep-disposal analogue. *Applied Geochemistry* 27, 1384. <https://doi.org/10.1016/j.apgeochem.2011.08.013>
- Tinseau, E., Bartier, D., Hassouta, L., Devol-Brown, I., Stammose, D., 2006. Mineralogical characterization of the Tournemire argillite after in situ interaction with concretes. *Waste Management*, 26, 7, 789-800. <https://doi.org/10.1016/j.wasman.2006.01.024>
- Trotignon, L., Devallois, V., Peycelon, H., Tiffreau, C., Bourbon, X., 2007. Predicting the long term durability of concrete engineered barriers in a geological repository for radioactive waste. *Physics and Chemistry of the Earth, Parts A/B/C* 32, 259. <https://doi.org/10.1016/j.pce.2006.02.049>
- Turrero, M.J., Cloet, V., 2017. FEBEX-DP Concrete ageing, concrete/bentonite and concrete/rock interaction analysis. *Nagra Arbeitsbericht NAB 16-18*, 5430 Wettingen Switzerland, p. 282. <http://www.grimseil.com/gts-phase-vi/febex-dp/febex-dp-literature-publications>
- Villar, M., Fernández, A., Rivas, P., Lloret, A., Daucausse, D., Montarges-Pelletier, E., Devineau, K., Villieras, F., Hynková, E., Cechova, Z., 2006. FEBEX Project: Final Report: Post-mortem Bentonite Analysis. ENRESA, Madrid. Spain



- Villar, M.V., Lloret, A., 2004. Influence of temperature on the hydro-mechanical behaviour of a compacted bentonite. *Applied Clay Science* 26, 337. <https://doi.org/10.1016/j.clay.2003.12.026>
- Villar, M.V., Martín, P.L., Bárcena, I., García-Siñeriz, J.L., Gómez-Espina, R., Lloret, A., 2012. Long-term experimental evidences of saturation of compacted bentonite under repository conditions. *Engineering Geology* 149-150, 57. <https://doi.org/10.1016/j.enggeo.2012.08.004>
- Walling, S.A., Provis, J.L., 2016. Magnesia-Based Cements: A Journey of 150 Years, and Cements for the Future? *Chemical Reviews* 116, 4170. <https://doi.org/10.1021/acs.chemrev.5b00463>
- Webb, P.A., Orr, C., 1997. Analytical methods in fine particle technology. Micromeritics Instrument Corp
- Williams L. A., Parks G. A., Crerar D. A., 1985. Silica Diagenesis, I. Solubility Controls. *SEPM Journal of Sedimentary Research*, 55, 301-311. [doi.org/10.1306/212F86AC-2B24-11D7-8648000102C1865D](https://doi.org/10.1306/212F86AC-2B24-11D7-8648000102C1865D)